4230 *Macromolecules* **2010**, *43*, 4230–4239
DOI: 10.1021/ma100391u

Macromolecules
ARTICLE

Structure and Gas Barrier Properties of Poly(propylene-*graft*-maleic anhydride)/Phosphate Glass Composites Prepared by Microlayer Coextrusion

Mohit Gupta, Yijian Lin, Taneisha Deans, Eric Baer, Anne Hiltner, and David A. Schiraldi*

Department of Macromolecular Science and Engineering and NSF Center for Layered Polymeric Systems, Case Western Reserve University, Cleveland, Ohio 44106

Received February 18, 2010; Revised Manuscript Received March 26, 2010

ABSTRACT: Alternating $(A-B-A)_n$ polymer films with individual layer thicknesses in the 3−25 μm range were produced using a robust layer multiplying coextrusion process. Such a film with layers of a poly(propylene-graft-maleic anhydride) (PPgMA) alternating with layers of PPgMA containing a phosphate glass (Pglass) upon biaxial orientation exhibited percolation of high barrier filler platelets resulting in reduction in gas permeation by two to 3 orders of magnitude. This unprecedented reduction in oxygen permeability was attributed to the high volume fraction of highly aligned Pglass platelets in the polymer matrix resembling a brick wall microstructure. Biaxially oriented films with 20 vol % Pglass content exhibited a microstructure resembling alternating organic and inorganic layers, a close replica of natural biocomposites. Structural models for permeability indicated that enhanced barrier resulted from increased tortuosity of the diffusion pathway provided by the aligned high aspect ratio platelets. Aspect ratios ranging from 40 to 175 were calculated by fitting the experimental data to diffusion models. Mechanical tests revealed that the presence of Pglass platelets increased the modulus of the multilayer composites by as much as 2×, without any considerable loss in ductility. The improvement in mechanical properties was ascribed to the high aspect ratio of the oriented Pglass platelets. Biaxially oriented films conditioned at high relative humidity (97% RH) maintained their high oxygen barrier properties. With an optical transparency between 60 and 85%, and good flexibility, these films stood out as good candidates for a variety of packaging applications.

Introduction

Polymers are currently used in a wide variety of barrier applications ranging from food and beverage packaging to electronic packaging systems necessary for flexible displays. Organic light emitting diodes (OLEDs) using plastic substrates are expected to provide a means of producing next-generation flat-panel displays that are thin, lightweight, and flexible. The use of transparent polymer films for encapsulating such displays is limited due to their unacceptably high permeation rates for oxygen and water.[1−3] Few thin films, that possess the combination of flexibility, transparency, gas barrier, thermal stability, and mechanical strength, have been reported to date.[4−7]

Incorporation of solid inorganic fillers with high aspect ratio has been widely examined as an approach to improve gas barrier properties of polymers. The decrease in gas permeability in such systems is known to be a function of the aspect ratio of the inclusions, their volume fraction and orientation. Alignment of overlapping platelet particles can greatly increase the diffusion distance and barrier properties by creating a tortuous path for the diffusing species, but with a significant loss in optical transparency and ductility.[8−11] Incorporating such fillers in large amounts also complicates processing due to the inherent increase in melt viscosity.

Phosphate glasses possessing low glass transition temperatures (T_g) which display both water resistance and chemical durability have been described in the literature[12,13] These phosphate glasses are fluidic over a range of temperatures that includes the melt processing temperature of many polymers. It is therefore possible to process these inorganic glasses with organic polymeric materials using conventional processing methodologies to yield composite materials containing phosphate glass loadings as high as 50−60 vol %.[14,15] In a previous study, the gas barrier properties of monolayer compression molded structures of poly(propylene-*g*-maleic anhydride) PPgMA containing Pglass were evaluated. The Pglass dispersed as spherical droplets in the polymer matrix was deformed into high aspect ratio platelets during the biaxial stretching process. A 2 orders of magnitude improvement was achieved compared to the unoriented bulk polymer.[16] Unlike clay-based nanocomposites, where a high degree of exfoliation and orientation of the clay platelets at filler concentrations greater than 3−5 vol % is very challenging, the present approach was amenable to high loadings of the Pglass filler without any loss of platelet orientation.

The layer multiplying coextrusion technique employed in the present work enables the production of layered films with tens or thousands of alternating layers of two or three different polymers with individual layer thicknesses in the 10 nm to 100 μm range and various arrangements.[11,17,18] Using this technology, polymers with widely dissimilar solid state morphologies and properties can be combined into unique layered and gradient structures. Micro and nano layers with up to 4096 layers and individual layer thicknesses less than 20 nm have been successfully produced with this system. As the layer thickness approaches the micro and nanometer length scales, useful and interesting changes in gas transport,[11] mechanical,[17] and optical[18] properties occur. This technology therefore offers an attractive approach for creating designed architectures from particulate-filled polymers such as alternating filled/unfilled layers with varying thickness and composition. Coupling of carefully chosen inorganic/organic barrier

*Corresponding author. E-mail: david.schiraldi@case.edu. Telephone: 216-368-4243. Fax: 216-368-4202.

 Published on Web 04/07/2010

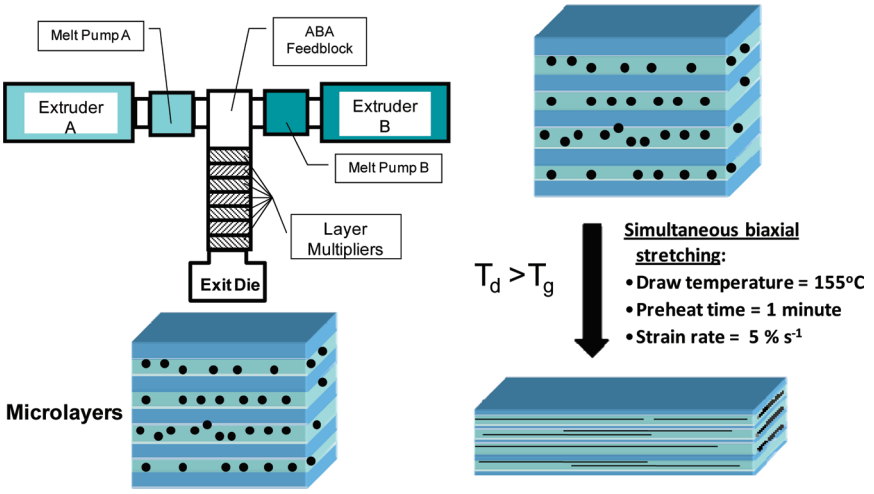

Figure 1. Schematic of the multilayer coextrusion process used to produce alternating $(ABABA)_n$ microlayers of Pglass filled and unfilled PPgMA which are then biaxially oriented to produce Pglass microplatelets.

systems with multilayering technology offers the potential for generating tens or hundreds of individual, high aspect ratio barrier domains through which oxygen, carbon dioxide, water vapor, or any permeant of interest would have to traverse. To take advantage of this, the present work aims to utilize low T_g phosphate glasses as impermeable fillers in multilayered polymer structures. These multilayered structures deploy layers of a PPgMA/Pglass composite alternating with layers of unfilled polymer. The layers were extruded in a $(ABA)_n$ arrangement with outer layers A of PPgMA. The number of layers (N) were determined by the number of multiplier elements (m) as $N = 2^{m+1}$. The Pglass, dispersed as spherical droplets in the filled layers, can then be deformed under biaxial orientation into high aspect ratio platelets. A schematic of the process is shown in Figure 1.

This approach we believe should lead to a highly regular and aligned regime of Pglass platelets unique to these multilayer structures giving us significant improvement in gas barrier properties. In this study, highly impermeable composite films prepared using conventional melt processing methodologies are reported. These films exhibit an improvement of 5−10 times in oxygen barrier compared to monolayer compression molded structures in addition to good transparency and flexibility. Composite gas transport models explain the observed 2−3 orders of magnitude reduction in oxygen transport compared to the neat polymer.

Experimental Section

Materials. Poly(propylene-*graft*-maleic anhydride) (PPgMA) with 0.2 wt % maleic anhydride (grade PB 3002) was provided by (Chemtura Corporation) with a density and melt flow index (MFI) of 0.91 g cm^{-3} and 7 g $(10\ min)^{-1}$ (ASTM D 1238) respectively. Reagent grade tin fluoride (SnF_2), tin oxide (SnO) and ammonium dihydrogen phosphate ($NH_4H_2PO_4$) were all used as received (Aldrich Chemical Co.).

Glass Preparation. The phosphate glasses (Pglass) were prepared on a 250 g scale. The ingredients were carefully weighed and added into a closed jar to form Pglass with a batch molar composition of 50% SnF_2 + 20% SnO + 30% P_2O_5. The ingredients were tumble mixed for 25−30 min to produce a uniform mixture and then transferred to a 300 mL capacity vitreous carbon crucible. The crucible was placed, uncovered, into a Thermolyne FA 1635 muffle furnace at 450 °C for 70 min. Fluid melts obtained using this procedure were quenched onto a stainless steel plate and annealed by placing in the oven at approximately 20 °C above the T_g for about 90 min.[12,13] This process resulted in a Pglass with a density of 3.65 ± 0.01 g cm^{-3} and a T_g of 118 ± 2 °C.

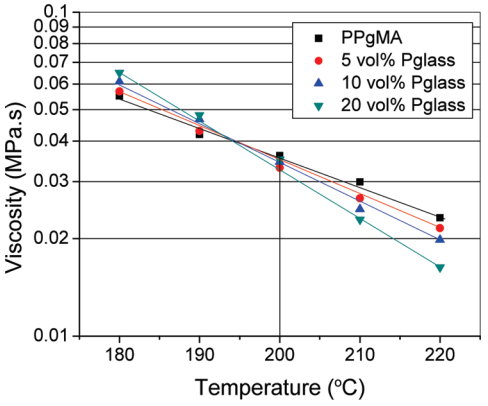

Figure 2. Melt flow index (MFI) data for neat PPgMA and PPgMA/Pglass composites.

Composite Preparation. The composites containing 10, 20, and 40 vol % Pglass were prepared using a Thermo-Haake Rheomix 3000 batch mixer equipped with roller rotors. The PPgMA and Pglass were batch mixed at 210 °C at a rotor speed of 60 rpm for 8 min, then collected as pieces about 2 mm thick and 100 mm ×100 mm across. The PPgMA was dried in a vacuum oven at 80 °C for at least 24 h prior to melt blending. The Pglass was ground to fine powder ground using an IKA M20 mill and stored in a desiccator before use in order to prevent any moisture absorption.

Microlayering. Films with 17, 33, 65, and 129 alternating layers were extruded using a layer multiplying coextrusion system described previously.[11,17,18] The layers were extruded in a $(ABA)_n$ arrangement with outer layers A of PPgMA. The number of layers (N) was determined by the number of multiplier elements (m) as $N = 2^{m+1}$. The melt from the final multiplier was spread through a 14-in. film die that had adjustable lips and a rectangular spreading geometry onto a laboratory-scale chill roll (Randcastle Extrusion Systems; Cedar Grove, NJ) maintained at 80 °C. The speed of the chill roll was used to control the overall film thicknesses; 350−400 μm films were extruded in each case. The extruder, multiplier elements and die temperatures were set to 200 °C to ensure matching viscosities of the two polymer melts (Figure 2). For this study equal volumetric flow rates were used.

Biaxial Orientation. Square specimens 85 mm × 85 mm were cut from the microlayered films, marked with a grid pattern, and

biaxially stretched in a Brückner Karo IV biaxial stretcher at 155 °C at an engineering strain rate of 5% s^{-1} based on the original specimen dimensions. The preheat time before stretching was fixed at 1 min. The sheets were simultaneously and equibiaxially drawn to a target draw ratio of 3 × 3. The actual draw ratio calculated from the change in separation of the parallel grid lines was found to be approximately 6 × 6, substantially higher than the target draw ratio. It was thought that uniformity was affected by uneven heating. Especially with the unusually low strain rate used, a slightly higher temperature in the center of the stretching chamber could have resulted in uneven drawing. Biaxial orientation reduced the film thickness to about 10 μm.

Morphological Analysis. In order to analyze the morphology of the composite materials before and after biaxial orientation, the films were embedded in epoxy and microtomed at room temperature using a glass knife. The samples were sputter coated with palladium. The morphology was observed using a Philips XL scanning electron microscope (SEM). SEM images were analyzed using Image-Pro Plus software in order to estimate the average diameter of the dispersed Pglass droplets. Three different images were analyzed for each composition and the values were averaged to obtain the reported results.

Oxygen Permeability. Oxygen flux $J(t)$ at 0% relative humidity, 1 atm and 23 °C was measured with a MOCON OX-TRAN 2/20. The permeant gas stream was diluted with nitrogen to achieve a 2% oxygen concentration in order to avoid exceeding the detector capability of the instrument. Permeability was obtained from the steady flux J_0 according to

$$P = J_o l/p \tag{1}$$

where p is the oxygen pressure and l is the film thickness. To study the effect of relative humidity (RH) on oxygen permeability, the biaxially oriented films were conditioned for a period of 1 month at 97% RH. The 97% RH was maintained with a saturated potassium sulfate (K_2SO_4) aqueous solution in accordance with ASTM E 104-85. Oxygen permeability was measured on conditioned films at 23 °C with the MOCON Oxtran2/20 with the RH adjusted to 97%. Two films prepared under the same conditions were tested to obtain the average permeability.

Positron Annihilation Lifetime Spectroscopy (PALS). PALS was performed using the fast−fast coincident method with a time resolution of 230 ps, at a count rate of 10^6counts/h. A 30 μCi ^{22}NaCl positron source was sandwiched between two identical stacks of biaxially oriented films (65 layers), each with thickness of 0.5 mm and 1 × 1 cm^2 area. The measurements were carried out at ambient laboratory conditions. A total of 15 PALS spectra were collected for each specimen and were tested against two and three component fits using the PATFIT program. The shortest lifetime component (τ_1) and the corresponding intensity (I_1) are attributed mainly to the annihilation of parapositronium (p-Ps). The intermediate lifetime component (τ_2) and the corresponding intensity (I_2) are attributed mainly to the annihilation of free positrons. The longest lifetime component τ_3 and the corresponding intensity I_3 are usually ascribed to the orthopositronium (o-Ps) pickoff annihilation and exhibit correlations to the size and concentration of the free volume holes, respectively. The average free volume hole radius (R) can be calculated from the o-Ps lifetime (τ_3) using the semiempirical equation[19,20]

$$\tau_3 = 0.5\left[1 - \frac{R}{R_o} + \frac{1}{2\pi}\sin\left(\frac{2\pi R}{R_o}\right)\right]^{-1} \tag{2}$$

where $R_o = R + \Delta R$ and (ΔR = 1.66 Å). Using the value of R, the mean free volume hole size (V_f) is calculated as $V_f = (4/3)\pi R^3$. For PPgMA and PPgMA/Pglass composites, optimal fits were obtained to three components with variance smaller than 1.20.

Mechanical Properties. Mechanical properties of both the oriented and unoriented microlayered films were evaluated in uniaxial tension on an Instron 5565 universal tester. Dog bone shaped specimens were punched from the films using an ASTM-D638 V punch tool and were tested at ambient temperature at a strain rate of 10%/min. Modulus values calculated from the initial slope of the stress−strain curve at 1% strain are reported. Three specimens were tested for each composition and the values were averaged to obtain the reported results.

Optical Clarity. Light transmission of the biaxially oriented films was measured using an ultraviolet−visible spectrometer (Ocean Optics, Dunedin, FL). The films were sandwiched between two glass slides to prevent curving, and then placed between the light source and light detector. Mineral oil with refractive index of 1.500 was spread on both surfaces of the film. The transmitted intensity at 633 nm wavelength was taken to calculate the light transmission as

$$T\ (\%) = \frac{T_{633}}{T^{\circ}_{633}} \times 100 \tag{3}$$

where T°_{633} is the light transmission at 633 nm with two glass slides as the reference and T_{633} is the total light transmission at 633 nm of the two glass slides with the film in between them. The measurement was performed at three different locations on each film and the average and standard deviation are reported.

Results and Discussion

PPgMA was used as the polymer matrix as it demonstrated better compatibility with the Pglass than polypropylene homopolymer (PP). The hydrogen bonding between the hydroxyl groups on the glass surface and the maleic anhydride group in PPgMA led to improved interfacial adhesion and resulted in smaller dispersed Pglass droplet size when PPgMA was used as the polymer matrix. The PPgMA/Pglass 90/10, 80/20 and 60/40 v/v composites were obtained by melt mixing in a Haake batch mixer. These composites formed the "B" layers of alternating $(A-B-A)_n$ multilayered films. The Pglass was dispersed as spherical droplets in the polymer matrix after melt mixing. The SEM images of these composites were analyzed using image analysis software in order to estimate the average diameter of the dispersed droplet phase in the composites. The average particle size was about 1.9 ± 0.6, 2.5 ± 1.1, and 3.5 ± 1.5 μm for the 90/10, 80/20, and 60/40 v/v composites, respectively. The increase in Pglass droplet size with increasing Pglass volume concentration in the polymer composites was attributed to the coalescence of Pglass particles during melt blending.

Layer-multiplying coextrusion produced microlayer films with alternating layers of Pglass-filled PPgMA and unfilled PPgMA. The layer thickness was varied by changing the number of coextruded layers while keeping the overall film thickness constant. Multilayered films with 17, 33, 65, and 129 layers and with nominal layer thicknesses of approximately 24, 12, 6 and 3 μm were obtained. The composition ratio A/B was kept constant at 50/50 v/v resulting in microlayered films with final Pglass concentrations of 5, 10, and 20 vol %. The SEM images in Figure 3 show the cross sections of the 17, 33, 65, and 129 layers films with a total Pglass content of 10 vol % (20 vol % Pglass in the filled layers). The unfilled and filled layers are readily distinguished even in the case of 129 layers where the Pglass droplet size was comparable to the layer thickness. The Pglass particles were uniformly distributed in the filled layers and the Pglass particle orientation/alignment in the filled layers seemed to significantly improve with increasing the number of layers.

In order to deform the dispersed spheres into high aspect ratio platelets, biaxial orientation of the microlayered films was carried out using a previously established procedure.[16] The target draw

ratio of 3 × 3 was chosen based on previous results where the largest reduction in permeability was obtained by stretching to a target draw ratio of 3 × 3. Stretching the composites to higher draw ratios resulted in some increase in permeability which was attributed to breakup of the platelet-shaped particles and possibly to some cavitation that occurred during stretching.[16] The SEM images of the film cross sections after biaxial orientation revealed a well-defined layered structure with an exceptionally high degree of Pglass platelets alignment, leading to an extremely tortuous path for diffusing gas molecules (Figure 4).

Oxygen Permeability. It is well understood through theoretical models as well as experimental studies that the barrier properties of a polymer containing a less permeable filler are strongly influenced by the final morphology. In general, the lowest permeability is obtained with continuous layers arranged perpendicular to the flux direction. On the other hand, a droplet morphology is associated with the highest permeation. Oriented and high aspect ratio platelets can approach the performance of continuous layers due to increased area fraction and increased tortuosity to permeants. The oxygen permeability data for the microlayered films before and after biaxial orientation are summarized in Table 1. The presence of spherical Pglass droplets decreased the $P(O_2)$ by 20−30% whereas high aspect ratio Pglass platelets reduced the $P(O_2)$ by 2−3 orders of magnitude.

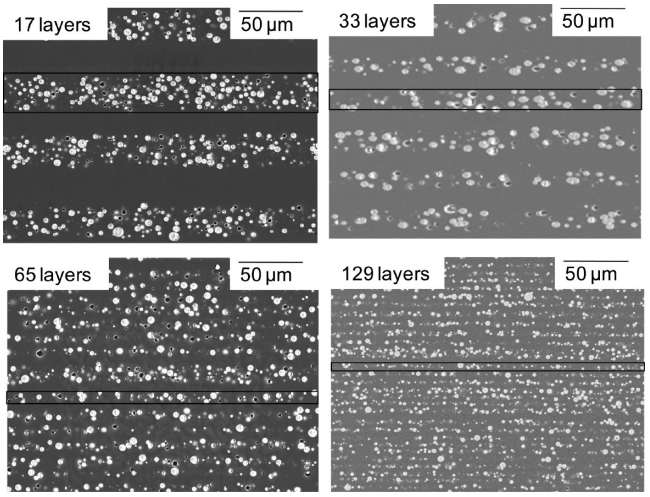

Figure 3. SEM images of microlayered film with 10 vol % Pglass across the film cross section.

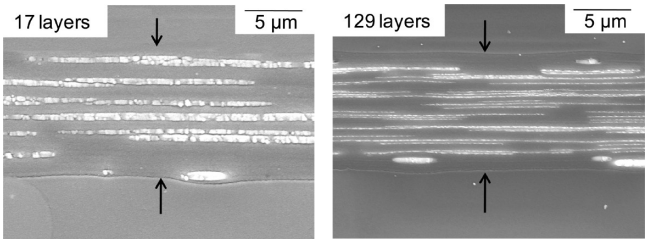

Figure 4. SEM images of biaxially oriented microlayered film with 10 vol % Pglass across the film cross section. The arrows define the cross section of the film.

The gas permeability of an ABABA layered assembly[11] can be calculated as

$$P_{AB} = \left(\frac{\phi_A}{P_A} + \frac{1-\phi_A}{P_B}\right)^{-1} \quad (4)$$

where φ_A is the volume fraction of the unfilled PPgMA layer, P_A is the oxygen permeability of the unfilled PPgMA layer and P_B is the oxygen permeability of the PPgMA/Pglass composite layer. Because of the presence of spherical Pglass droplets in the as-extruded microlayered films it was anticipated that the permeability P_B of the filled layer would be described by the Maxwell model for randomly dispersed spherical particles of lower permeability in a continuous matrix of higher permeability[21]

$$\frac{P_B}{P_m} = 1 + \frac{3\phi_{\text{Pglass}}}{\left[\frac{(P_{\text{Pglass}}/P_m)+2}{(P_{\text{Pglass}}/P_m)-1}\right] - \phi_{\text{Pglass}}} \quad (5)$$

where P_{Pglass} and P_m are the permeabilities of the dispersed Pglass particles and the PPgMA matrix, respectively, and ϕ_{Pglass} is the volume fraction of Pglass in the filled layer. Assuming Pglass to be impermeable ($P_{\text{Pglass}} = 0$) and taking P_m from Table 1 as 0.87 barrer, the permeability of the filled layer was calculated from eq 5. Combining the results with eq 4 satisfactorily describe the permeability of the as-extruded films. It is also consistent with eqs 4 and 5 that permeability of the as-extruded films depended only on the Pglass content, and not on the number of layers or layer thickness.

The slight decrease in $P(O_2)$ of neat PPgMA films from 0.86 ± 0.02 barrer to 0.65 ± 0.03 barrer after biaxial orientation to a draw ratio of 3 × 3 was attributed to lower diffusivity due to tightening of amorphous tie chains and was consistent with previous reports for biaxially stretched isotactic PP.[22] Transformation of the spherical Pglass particles into platelets by biaxial stretching increased the tortuosity of the diffusion pathway and remarkably decreased the permeability of the composite films. If the particles are platelet-shaped with aspect ratio α and oriented perpendicular to the flux direction, permeability models including of Nielsen[23]

$$\frac{P}{P_m} = \frac{1-\phi_{\text{Pglass}}}{1+\alpha\frac{\phi_{\text{Pglass}}}{2}} \quad (6)$$

and Cussler[24]

$$\frac{P}{P_m} = \frac{1-\phi_{\text{Pglass}}}{1+\left(\alpha\frac{\phi_{\text{Pglass}}}{2}\right)^2} \quad (7)$$

can be applied. The dependence on the square of both α and φ in eq 7 is due to both the increased distance for diffusion

Table 1. Oxygen Permeability of Unoriented and Biaxially Oriented Microlayered Films with Different Number of Layers

	$P(O_2)$ (barrer)							
	17 layers		33 layers		65 layers		129 layers	
	1 × 1	3 × 3	1 × 1	3 × 3	1 × 1	3 × 3	1 × 1	3 × 3
PPgMA control	0.88 ± 0.02	0.65 ± 0.03	0.87 ± 0.01	0.65 ± 0.03	0.86 ± 0.01	0.62 ± 0.02	0.86 ± 0.02	0.64 ± 0.03
5 vol % Pglass	0.81 ± 0.01	0.32 ± 0.02	0.80 ± 0.01	0.19 ± 0.02	0.80 ± 0.01	0.13 ± 0.01	0.80 ± 0.01	0.11 ± 0.01
10 vol % Pglass	0.73 ± 0.03	0.13 ± 0.02	0.74 ± 0.02	0.029 ± 0.004	0.71 ± 0.02	0.013 ± 0.002	0.72 ± 0.02	0.012 ± 0.001
20 vol % Pglass	0.60 ± 0.03	0.028 ± 0.004	0.60 ± 0.02	0.006 ± 0.001	0.59 ± 0.03	0.002 ± 0.0005	0.62 ± 0.03	0.0017 ± 0.0003

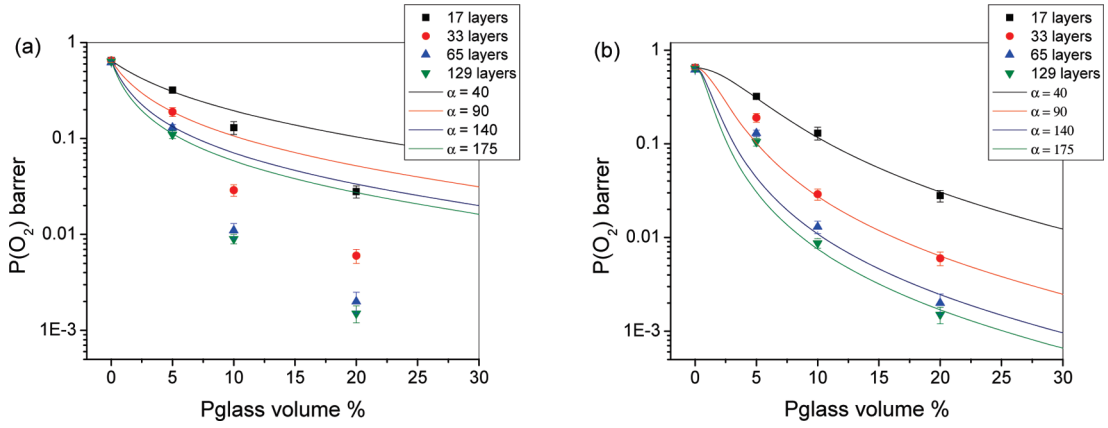

Figure 5. Experimental data for oxygen permeability versus volume fraction of Pglass for biaxially oriented composite films with various fits according to (a) Nielsen and (b) Cussler equations.

Table 2. Water Sorption and Oxygen Permeability Data for Biaxially Oriented Films with 65 Layers Conditioned at 23°C/97% RH for 1 month

	water sorption (wt %)	$P(O_2)$ (barrer), 0% RH	$P(O_2)$ (barrer), 97% RH	drop in $P(O_2)$ (%)
PPgMA control	0.30 ± 0.02	0.62 ± 0.02	0.56 ± 0.02	10 ± 2
5 vol % Pglass	0.60 ± 0.05	0.13 ± 0.01	0.11 ± 0.01	12 ± 5
10 vol % Pglass	0.8 ± 0.05	0.013 ± 0.002	0.011 ± 0.001	15 ± 2
20 vol % Pglass	1.70 ± 0.2	0.002 ± 0.0005	0.0016 ± 0.0004	22 ± 3

and reduced cross sectional area between the platelets. Increasing the platelet volume fraction leads to increasing overlap between platelets, causing reduction in the cross section area between the platelets through which the diffusion is occurring. This overlap leads to repeated multiple scattering of the penetrant gas molecule between close pair of platelets, thereby increasing the tortuosity of the diffusion pathway and a change in diffusion mechanism from Nielsen to Cussler type.

The permeability data for the stretched films were fit to the Nielsen and Cussler models using the aspect ratio α as the only adjustable parameter. Equation 6 satisfactorily described the results for the lower Pglass loadings (5 vol % Pglass) with a particle aspect ratio α that increased from 40 to175 as the number of layers increased Figure5a. On the other hand, $P(O_2)$ of the composites with higher Pglass content (10 and 20 vol % Pglass) was considerably lower than the prediction from eq 6. When the results for these films were compared against the prediction from eq 7 using the aspect ratios extracted from the Nielsen analysis, good agreement was obtained, 5b. The aspect ratios obtained by fitting the permeability data were consistent with the platelet dimensions observed in the SEM images of the film cross section. The increase in aspect ratio with increasing number of layers was mainly attributed to a decrease in the thickness of Pglass platelets as the layers became thinner. Confining the Pglass in thinner layers prevented the lateral coalescence of Pglass particles during biaxial stretching. Whereas the length of the platelets was approximately 15−20 μm in all the films, the thickness of the platelets decreased from 350 to 80 nm as the number of layers increased from 17 to 129. Biaxially oriented films with 20 vol % Pglass content exhibited a microstructure resembling alternating organic and inorganic layers Figure 6. The layered platelet morphology provided an extremely tortuous pathway for the permeant gas.

A film with 17 layers (8 layers of Pglass composite) and 10 vol % Pglass brought about a 7× reduction in oxygen permeability compared to the unoriented PPgMA control. The same composition with 129 layers (64 containing Pglass) resulted in about a 70x reduction in oxygen permeability to

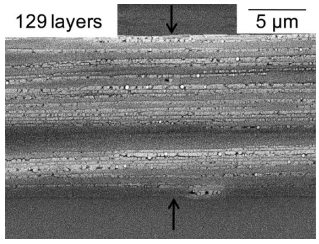

Figure 6. Cross section of a biaxially oriented film with 20 vol % Pglass. The arrows define the cross section of the film.

0.012 barrer. The value compared favorably with some of the most widely used oxygen barrier polymers such as poly(ethylene terephthalate) (PET) (0.036 barrer)[25] and Nylon-6,6 (0.010 barrer).[26] When the concentration of the Pglass in the film cross section is increased to 20 vol %, the permeability decreased by almost another order of magnitude to 0.0017 barrer, a value similar to that of aromatic polyamides based on hexamethylenediamine (Nylon MXD6) (0.002 barrer).[25]

Effect of Humidity. It is well-known that water has a significant effect on the gas barrier properties of most hydrophilic polymers. Water sorption at high relative humidity (RH) seriously compromises the gas barrier of hydrophilic polymers such as PEO, Nylon-6 and EVOH,[11,27,28] even the gas barrier performance of clay nanocomposites tends to deteriorate under humid conditions because of the hydrophilic nature of the clay.[29] Polypropylene demonstrates excellent moisture barrier, while phosphate glasses are documented to have low water durability. Hence, it was important to evaluate the effect of humidity on the gas barrier properties of the composite films. Water uptake and oxygen flux were recorded for biaxially oriented composites films with 65 layers, after they were conditioned at 97% RH for 1 month. The results are shown in Table 2. The water uptake increased with the Pglass content, with a maximum uptake of approximately 1.7 wt % for the film with 20 vol % Pglass content. Interestingly, the oxygen permeability decreased after the films were conditioned. A decrease in oxygen permeability for nylon-6 (0−50% RH),[27]

PET (0−100% RH),[30] and Nylon MXD6 (0−70% RH),[31] has been demonstrated before. The results were explained on the basis of absorbed water occupying part of the static free volume and thereby reducing the oxygen solubility.

A common method for obtaining the gas solubility is to extract the diffusivity D from the nonsteady state flux curve and calculate $S = P/D$. However, the biaxially oriented films were very thin, about 10 μm, and in the measurements the steady state flux was reached too rapidly to record the nonsteady state region. Instead, PALS was used to probe changes in free volume due to moisture sorption. PALS is an important and widely used technique for probing the sub-nanometer-sized local free volume in polymeric materials and composites, and has recently been used to study moisture absorption/desorption in polymers.[32−34] Figure 7 shows the spectra of Pglass, biaxially oriented PPgMA, and the biaxially oriented composite with 20 vol % Pglass. The Pglass lifetime spectra decayed very rapidly and was resolved into two components (τ_1 and τ_2). Most of the decay was related to the shortest lifetime component (τ_1 = 0.2 ns and I_1 = 65%), with less intermediate lifetime contribution (τ_2 = 0.56 ns and I_2 = 35%) and no longer lifetime contribution, which agreed well with the reported values for certain oxide based glasses.[35] Positrons annihilated very rapidly due to the low concentration of defects and the absence of holes for the o-Ps formation, which was consistent with the excellent gas barrier properties of these glasses. The decay curves were similar for neat PPgMA and PPgMA/Pglass composite materials. The lifetime spectra were resolved into three components, the o-Ps intensity (I_3) of long-lived component τ_3 was about 15%, indicating that an appreciable fraction of the positrons entering the sample resulted in the formation of o-Ps in the free volume holes of the PPgMA. The effect of volume fraction of Pglass on the o-Ps lifetime and intensity is shown in Figure 8, parts a and b. I_3 was found to be almost independent of the Pglass content confirming o-Ps are formed only in the PPgMA phase. The increasing volume fraction of Pglass resulted in higher τ_3 or free volume hole size (V_f) in the dry films. The increase in τ_3 was attributed to formation of large free volume cavities at the interface between the polymer and Pglass phase. Similar results have been reported by Chen et al.[36] and Winberg et al.[37] for polymer composites based on silica and clay, respectively. Both τ_3 and I_3 decreased for the films conditioned at 97% RH. The effect on τ_3 and I_3 became larger as the volume % of Pglass increased and paralleled an increase in water sorption (Table 2). The presence of absorbed moisture caused the o-Ps lifetime (τ_3) to decrease as water absorbed in large pre-existing holes resulted in a narrower distribution of holes accessible for o-Ps formation. Similarly, holes occupied by the water molecules were no longer available for o-Ps formation, resulting in a decrease in o-Ps intensity (I_3). This confirmed the hypothesis that absorption of water into the holes of the free volume was the primary reason for the drop in oxygen permeability.

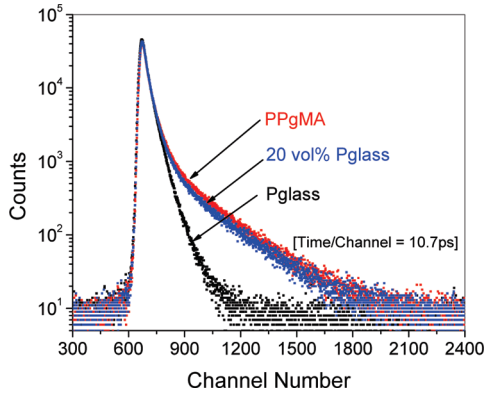

Figure 7. PALS lifetime spectra for Pglass and biaxially oriented PPgMA and PPgMA/Pglass composite with 20 vol % Pglass.

Mechanical Properties. The addition of inorganic fillers to polymers for increasing the modulus or stiffness via reinforcement mechanisms has been a widely studied phenomenon. Polymers filled with rigid inorganic particles display higher values of Young's modulus than unfilled polymers, but at the same time demonstrate a significant reduction in fracture strain.[6,7,38,39] In order to determine the effect of Pglass on the mechanical properties of the composite films, stress−strain behavior of both the unoriented and biaxially oriented multilayered films was investigated. Table 3 reports the tensile modulus, yield stress, fracture stress and elongation at break for the unoriented multilayered films. The presence of spherical Pglass led to a moderate improvement in the tensile modulus, while a small drop in the yield stress was recorded.

The stress−strain curve of the unfilled PPgMA was typical of ductile polymers with an engineering strain of approximately 350% before fracture. The stress−strain curves of the PPgMA/Pglass composites with up to 10 vol % Pglass were similar to that of the unfilled polymer. The composites showed ductile behavior with formation of a stable neck

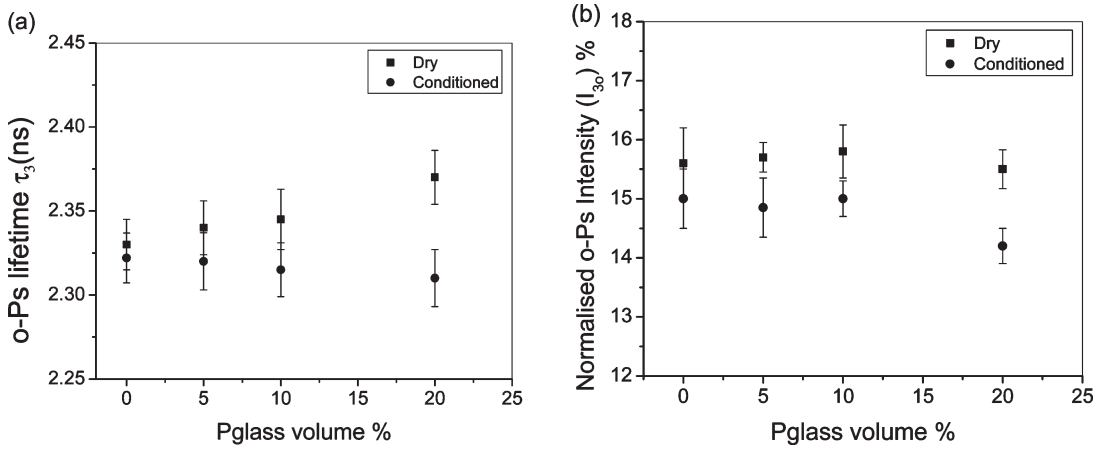

Figure 8. PALS data for biaxially oriented composite films with 65 layers as a function of Pglass volume fraction: (a) effect on o-Ps lifetime and (b) effect on o-Ps intensity normalized to PPgMA volume fraction according to $I_{3o} = I_3$/volume % PPgMA.

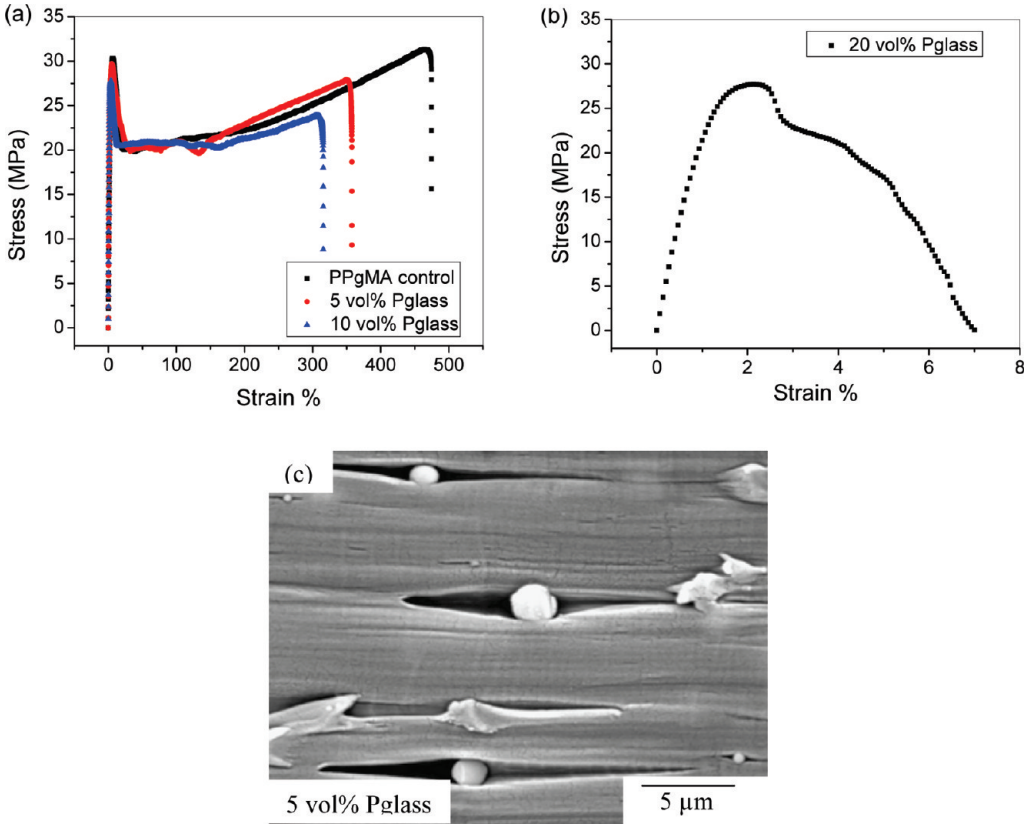

Figure 9. (a and b) Typical stress strain curves for as-extruded multilayered films with 65 layers and (c) SEM image of as-extruded 65 layers PPgMA/Pglass film strained to fracture and then cryogenically microtomed parallel to the direction of deformation.

Table 3. Summary of Tensile Properties of As-Extruded Microlayered Films

	modulus (GPa)	yield stress (MPa)	fracture stress (MPa)[a]	elongation at break (%)
PPgMA control (17 layers)	1.48 ± 0.02	31.6 ± 0.7	30.9 ± 0.3	320 ± 30
5 vol % Pglass (17 layers)	1.62 ± 0.04	29.6 ± 2.0	28.8 ± 1.9	280 ± 30
10 vol % Pglass (17 layers)	1.75 ± 0.03	28.9 ± 1.3	27.2 ± 2.1	230 ± 70
20 vol % Pglass (17 layers)	2.10 ± 0.02	27.5 ± 1.0	NA	8 ± 2
PPgMA control (33 layers)	1.46 ± 0.02	31.6 ± 0.5	30.9 ± 0.3	370 ± 30
5 vol % Pglass (33 layers)	1.65 ± 0.02	29.0 ± 1.0	28.2 ± 1.0	250 ± 30
10 vol % Pglass (33 layers)	1.75 ± 0.03	28.2 ± 1.5	27.0 ± 1.1	200 ± 30
20 vol % Pglass (33 layers)	2.15 ± 0.05	27.2 ± 1.0	NA	6 ± 2
PPgMA control (65 layers)	1.45 ± 0.02	32.5 ± 0.5	31.5 ± 1.0	400 ± 20
5 vol % Pglass (65 layers)	1.65 ± 0.02	29.9 ± 0.3	28.3 ± 1.9	300 ± 50
10 vol % Pglass (65 layers)	1.75 ± 0.02	29.0 ± 1.1	28.5 ± 2.4	230 ± 30
20 vol % Pglass (65 layers)	2.15 ± 0.05	28.2 ± 1.0	NA	5 ± 2
PPgMA control (129 layers)	1.45 ± 0.05	32.0 ± 1.0	31.5 ± 1.0	450 ± 50
5 vol % Pglass (129 layers)	1.68 ± 0.03	30.6 ± 0.4	29.8 ± 1.5	300 ± 50
10 vol % Pglass (129 layers)	1.78 ± 0.03	29.0 ± 1.0	28.0 ± 1.0	200 ± 50
20 vol % Pglass (129 layers)	2.1 ± 0.05	27.2 ± 0.8	NA	6 ± 2

[a] Normalized to PPgMA volume %.

(Figure 9, parts aand b). The fracture strain decreased as the filler content increased primarily due to the decrease in the length of the strain hardening region. For polymer composites, if particle debonding from the matrix occurs prior to plastic deformation of the matrix, usually the yield strength will decrease and relatively unhindered plastic deformation of the polymer matrix around the particles will lead to composites with relatively ductile behavior.[40] The debonding and void growth in the tensile samples sectioned along the stretching direction is shown in Figure 9c and was representative of all the composites with 5 and 10 vol % Pglass. The micrograph shows elongated voids that contain Pglass particles. The voids have the shape that would be expected if the polymer debonded and drew out around the particles, allowing the matrix to undergo the large local strain required in the necking process. As the Pglass volume fraction was increased to 20 vol %, the composites failed in a quasi-brittle manner as some level of plastic deformation preceded fracture even though the fracture strain dropped significantly. The fracture strain was only approximately 5% indicating that a neck formed but the neck was not strong enough to support drawing and fractured. This transitional behavior from ductile drawing to quasi-brittle fracture at low strains occurred when the amount of matrix material in the cross section dropped below the critical value needed to support the engineering draw stress.[40] The as-extruded PPgMA/Pglass

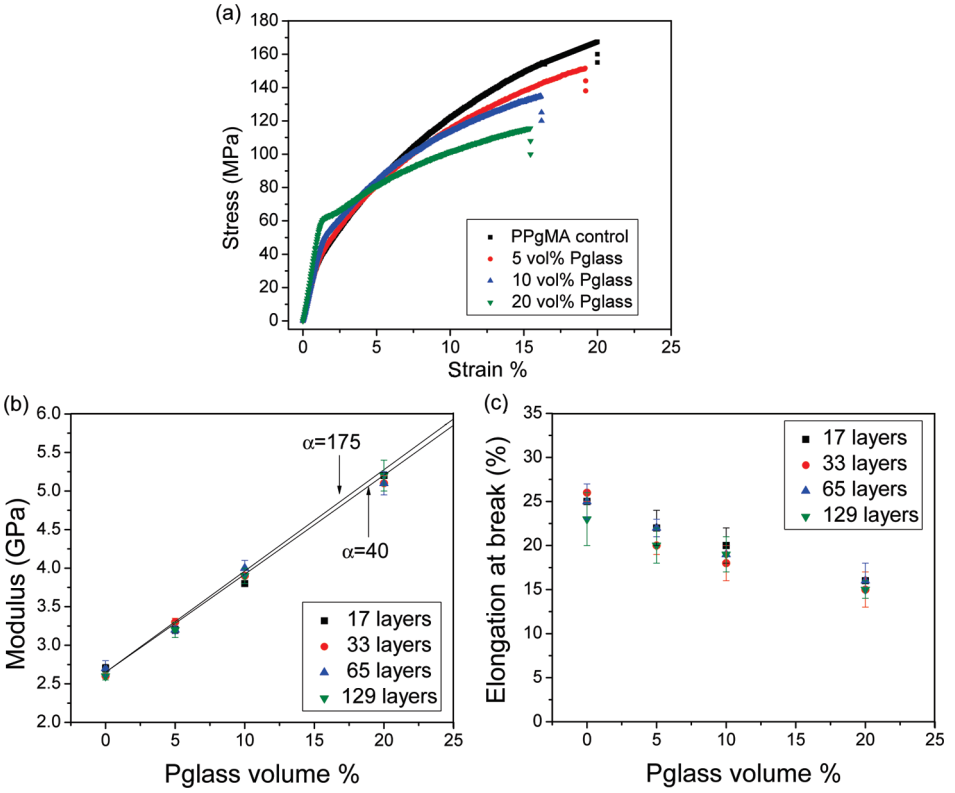

Figure 10. (a) Typical stress strain curves for biaxially oriented multilayered films with 65 layers. (b) Experimental modulus data for Pglass reinforced PPgMA and model predictions from eq 9 (solid lines) based on experimentally determined aspect ratio (α) and $E_f/E_m = 6$. (c) Dependence of elongation at break on the Pglass volume %.

composites with different number of layers demonstrated very similar mechanical properties.

Figure 10a shows the typical stress−strain behavior for the biaxially oriented films with 65 layers. The elongation at break for biaxially oriented films is considerably lower than that for as-extruded films. The drop in elongation at break is due to less potential for orientation in the sheets that have been stretched to a high draw ratio. The biaxially oriented films are already stretched approximately 6 × 6 times (actual draw ratio) and have gone through yielding during biaxial orientation The polymer chains are now already uncoiled and aligned. On the other hand, orientation of polymer chains during the biaxial orientation process led to an increase in tensile modulus of the neat PPgMA from 1.5 to 2.7 GPa. The presence of Pglass platelets led to a substantial improvement in the tensile modulus. The modulus of the composite films increased by a factor of 1.25−2.0× depending on the volume % of the Pglass in the composite without any significant loss of toughness as determined by the area under the stress−strain curve. A small reduction in the tensile strength of the composite films was recorded with the increasing volume fraction of Pglass and can be attributed to low interfacial compatibility at the organic−inorganic interface. The tensile modulus and elongation at break for the biaxially oriented composite films with different number of layers is shown in Figure 10, parts band c.

The Halpin−Tsai equation is widely used to estimate the reinforcement effects of a filler.[41] The modulus of composite materials reinforced by platelet shaped fillers can be expressed in the form

$$\frac{E_c}{E_m} = \frac{1 + 2\alpha\eta\phi_f}{1 - \eta\phi_f} \tag{8}$$

where

$$\eta = \frac{E_f/E_m - 1}{E_f/E_m + \alpha}$$

E_c is the composite modulus, E_f is the Pglass modulus, E_m is the matrix modulus, α is the aspect ratio, and φ_f is the volume fraction of Pglass. Good correlation between the theoretical and experimental values using values of 2.7 and 16 GPa for the matrix modulus and the filler modulus respectively (Figure 10b). When the aspect ratios are much larger than the ratio of filler to matrix modulus ($\alpha \gg E_f/E_m$) the Halpin−Tsai equation can be reduced to the form

$$E_c = E_f\phi_f + E_m(1 - \phi_f) \tag{9}$$

In this case, the effect of α on the composite modulus becomes negligible as can be seen from Figure 10b.

Optical Clarity. Optical properties of polyolefin films such as haze and transparency are of considerable importance in many packaging applications. Values for the % light transmission through 10 μm thick biaxially oriented films with 65 layers is presented in Figure 11a. Mineral oil with refractive index of 1.500 was spread on both surfaces of the film to smooth the film surface and eliminate light scattering from surface roughness. The biaxially oriented PPgMA control films exhibited excellent light transmission of almost 100%. With addition of Pglass, light transmission somewhat decreased from 85 to 60% depending on the volume fraction of Pglass in the composite. The loss of light transmission was attributed to bulk scattering due to refractive index mismatch between the polymer matrix and the Pglass filler. Addition of Pglass to PPgMA resulted in films with slight

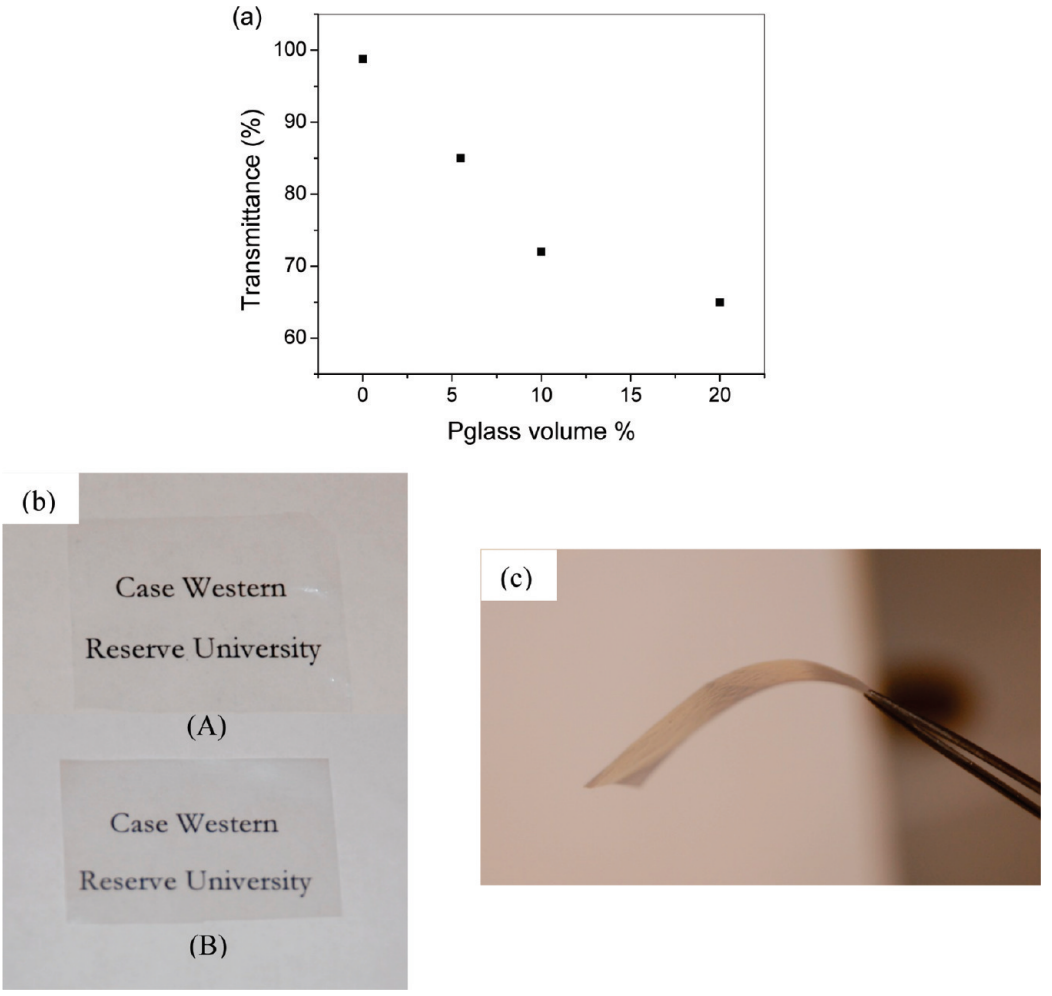

Figure 11. (a) Measured light transmission through biaxially oriented films with oil of matching refractive index on both surfaces. (b and c) Free standing 65 layer biaxially oriented films (A) PPgMA control (B) PPgMA/Pglass composite with 20 vol % Pglass showing transparency and good flexibility.

haziness; however, good overall see through clarity was still maintained (Figure 11b).

Conclusions

A new class of organic polymer/inorganic glass hybrids with property improvements that are impossible to achieve with classical polymer blends or composites has been developed. A layer multiplication coextrusion process was used to produce microlayered films of neat PPgMA alternating with layers of a PPgMA/Pglass composite. The Pglass, which was dispersed as spherical droplets in the filled layers, elongated into high aspect ratio platelets during the biaxial stretching process. Biaxially oriented films exhibited a brick wall type microstructure with highly aligned inorganic platelets in a ductile organic matrix. The oxygen barrier of PPgMA was significantly improved due to presence of Pglass platelets as impermeable inclusions, comparing favorably to some of the most widely used oxygen barrier polymers such as PET, Nylon6,6, and Nylon MXD6. Properly dispersed and aligned Pglass platelets proved to be very effective for increasing the composite modulus without sacrificing ductility. Films that were stiff (5 GPa) yet ductile (φ_b ~15%) were produced at a moderate inorganic volume fraction. This simple process resulted in a close replica of natural biocomposites with alternating organic and inorganic layers. The developed films are promising for a wide variety of advanced packaging applications because of their gas barrier properties, flexibility, transparency, mechanical strength and performance under humid conditions.

Acknowledgment. This research was supported by the National Science Foundation under Grant No. DMR 0423914.

References and Notes

(1) Groner, M. D.; George, S. M.; McLean, R. S.; Garcia, P. F. *Appl. Phys. Lett.* **2006**, *88*, 051907/1–051907/3.
(2) Burrows, P. E.; Graff, G. L.; Gross, M. E.; Martin, P. M.; Shi, M. K.; Hall, M.; Mast, E.; Bonham, C.; Bennett, W.; Sullivan, M. B. *Displays* **2001**, *22*, 65–69.
(3) *Plastics Packaging*; Selke, S. E. M., Culter, J. D., Hernandez, R. J., Eds.; Hanser Verlag: Munich, Germany, 2004.
(4) Ebina, T.; Mizukami, F. *Adv. Mater.* **2007**, *19*, 2450–2453.
(5) Tetsuka, H.; Ebina, T.; Tsunoda, T.; Nanjo, H.; Mizukami, F. *J. Mater. Chem.* **2007**, *17*, 3545–3550.
(6) Podsiadlo, P.; Kaushik, A. K.; Arruda, E. M.; Waas, A. M.; Shim, B. S.; Xu, J.; Nandivada, H.; Pumplin, B. G.; Lahann, J.; Ramamoorthy, A.; Kotov, N. A. *Science* **2007**, *318*, 80–83.
(7) Bonderer, L. J.; Studart, A. R.; Gauckler, L. J. *Science* **2008**, *319*, 1069–1073.
(8) Bissot, T. C. In *Barrier Polymers and Structures*; Koros, W. J., Ed.; American Chemical Society: Washington, DC, 1990; p 225.
(9) Sekelik, D. J.; Stepanov, E. V.; Nazarenko, S.; Schiraldi, D. A.; Hiltner, A.; Baer, E. *J. Polym. Sci., Part B: Polym. Phys.* **1999**, *37*, 847–857.
(10) Osman, M. A.; Mittal, V.; Lusti, H. R. *Macromol. Rapid Commum.* **2004**, *25*, 1145–1149.
(11) Wang, H. P.; Keum, J. K.; Hiltner, A.; Baer, E. *Macromolecules* **2009**, *42*, 7055–7066.
(12) Tick, P. A. *Phys. Chem. Glasses* **1984**, *25*, 149–154.
(13) Shaw, C. M.; Shelby, J. E. *Phys. Chem. Glasses* **1988**, *29*, 87–90.

(14) Frayer, P. D. US 6,103,810, **2000**.
(15) Urman, K.; Otaigbe, J. U. *Prog. Polym. Sci.* **2007**, *32*, 1462–1498.
(16) Gupta, M.; Lin, Y. J.; Deans, T.; Crosby, A.; Baer, E.; Hiltner, A.; Schiraldi, D. A. *Polymer* **2009**, *50*, 598–604.
(17) Im, J.; Hiltner, A.; Baer, E. In *High Performance Polymers*; Baer, E., Moet, A., Eds.; Hanser Verlag: Munich, Germany, 1991; p 175.
(18) Liu, R. Y. F.; Jin, Y.; Hiltner, A.; Baer, E. *Macromol. Rapid Commun*. **2003**, *24*, 943–948.
(19) Tao, S. J. *J. Chem. Phys*. **1972**, *56*, 5499–5510.
(20) Nakanishi, H.; Wang, S. J.; Jean, Y. C. In *Positron Annihilation Studies of Fluids*; Sharma, S. C., Ed.; World Science: Singapore, 1988; p 292.
(21) Barrer, R. M. In *Diffusion in Polymers*; Crank, J., Park, G. S., Eds.; Academic: New York, 1968; p 165.
(22) Lin, Y. J.; Dias, P.; Chen, H. Y.; Hiltner, A.; Baer, E. *Polymer* **2008**, *49*, 2578–2586.
(23) Nielsen, L. E. *J. Macromol. Chem*. **1967**, *A1*, 929–942.
(24) Cussler, E. L.; Stephanie, E. H.; William, J. W.; Rutherford, A. *J. Membr. Sci*. **1988**, *38*, 161–174.
(25) Hu, Y. S.; Prattipati, V.; Mehta, S.; Schiraldi, D. A.; Hiltner, A.; Baer, E. *Polymer* **2005**, *46*, 2685–2698.
(26) Jarus, D.; Hiltner, A.; Baer, E. *Polymer* **2002**, *43*, 2401–2408.
(27) Gavara, R.; Hernandez, R. J. *J. Polym. Sci., Part B: Polym. Phys*. **1994**, *32*, 2375–2382.
(28) Lagaron, J. M.; Gimenez, E.; Catala, R.; Gavara, R. *Macromol. Chem. Phys*. **2003**, *204*, 704–713.
(29) Jang, W. S.; Rawson, I.; Grunlan, J. C. *Thin Solid Films* **2008**, *516*, 4819–4825.
(30) Auras, R.; Harte, B.; Selke, S. *J. Appl. Polym. Sci*. **2004**, *92*, 1790–1803.
(31) Mitsubishi Gas Chemical America, Inc. Product Brochure. http://www.mgc-a.com.
(32) Dlubek, G.; Buchhold, R.; Hübner, Ch.; Nakladal, A. *Macromolecules* **1999**, *32*, 2348–2355.
(33) Simon, G. P. *Trends Polym. Sci*. **1997**, *5*, 394–400.
(34) Sanchez, V.; Lopez, R.; Fucugauchi, L. A.; Ito, Y. *J. Appl. Polym. Sci*. **1995**, *56*, 779–791.
(35) Sasaki, Y.; Ohkubo, H.; Inoue, K.; Tang, Z.; Hasegawa, M. *Radiat. Phys. Chem*. **2003**, *68*, 569–572.
(36) Chen, H. M.; Jean, Y. C.; James Lee, L.; Yang, J.; Huang, J. *Phys. Stat. Sol. C* **2009**, *6*, 2397–2400.
(37) Winberg, P.; Eldrup, M.; Pedersen, N. J.; van Es, M. A.; Maurer, F. H. J. *Polymer* **2005**, *46*, 8239–8349.
(38) Russo, G. M.; Simon, G. P.; Incarnato, L. *Macromolecules* **2006**, *39*, 3855–3864.
(39) Paul, D. R.; Robeson, L. M. *Polymer* **2008**, *49*, 3187–3204.
(40) Bazhenov, S.; Li, J. X.; Hiltner, A.; Baer, E. *J. Appl. Polym. Sci*. **1994**, *52*, 243–254.
(41) Halpin, J. C.; Kardos, J. L. *Polym. Engng. Sci*. **1976**, *16*, 344–352.